Clays and Clay Minerals, Vol. 55, No. 5, 481–490, 2007.

EXTENSIVE DICKITIZATION OF THE PERMO-TRIASSIC FLUVIAL SANDSTONES FROM THE EASTERN IBERIAN RANGE, SPAIN

J. D. MARTÍN-MARTÍN[1,*], D. GÓMEZ-GRAS[2], T. SANFELIU[3], M. THIRY[4], M. D. RUIZ-CRUZ[5] AND F. FRANCO[5]

[1] Department of Earth Sciences, Uppsala University, SE-75236 Uppsala, Sweden
[2] Unitat de Petrologia i Geoquímica, Facultat de Ciències, Universitat Autònoma de Barcelona, 08193 Bellaterra, Spain,
[3] Departament de Ciències Experimentals, Universitat Jaume I, 12080 Castelló, Spain
[4] Centre de Géociences, École des Mines de Paris, 77305 Fontainebleau Cedex, France
[5] Departamento de Química Inorgánica, Cristalografía y Mineralogía, Universidad de Málaga, 29071 Málaga, Spain

Abstract—Diagenetic kaolin minerals are very common in the Permo-Triassic succession from the SE Iberian Range, Spain. The morphology and crystal structure of kaolin minerals has been examined in four size fractions (<1 μm, <2 μm, <6.3 μm and <20 μm) of sandstone samples by means of scanning electron microscopy, X-ray diffraction, infrared spectroscopy, differential thermal analysis and thermogravimetry. Experimental data reveal that dickite is the dominant kaolin-type mineral in the entire range of size fractions, whereas small amounts of kaolinite coexists with dickite in all size fractions. Dickite appears typically as booklets of pseudo-hexagonal plates with blocky habit. The increase in size fraction is concomitant with the increase in the amount of dickite and the progressive improvement of its structural order. The extensive dickitization is attributed to the high paleogeothermal gradient recorded in the studied area and the increase in H^+, presumably resulting from the flux of organic acids derived from the underlying Carboniferous rocks and/or the late Permian succession. These conditions are more likely to be associated with the late Cretaceous post-rift thermal stage of the eastern Iberian Basin. Lately, during the maximum burial depth, the fine crystalline kaolin minerals were slightly illitized. Given the very small feldspar content in the studied sequence, the results reflect the important contribution of mica alteration to the early diagenetic formation of kaolinite as well as the late conversion to dickite.

Key Words—Crystal Structure, Diagenesis, Dickite, Kaolinite, Morphology, Paleogeothermal Gradient, Permian, Sandstones, Triassic.

INTRODUCTION

Diagenetic formation of dickite has frequently been described during recent decades, mostly in relation to the widespread occurrence of this mineral in sandstone reservoirs from the North Sea (Sommer, 1975; Jourdan *et al.*, 1987; Ehrenberg *et al.*, 1993; McAulay *et al.*, 1994; Lanson *et al.*, 1996; Beaufort *et al.*, 1998) and in Permian and Triassic sediments from other basins (Platt, 1993; Ruiz-Cruz and Moreno-Real, 1993; Morad *et al.*, 1994; Ruiz-Cruz and Andreo, 1996). According to those authors, the early diagenetic vermicular kaolinite is replaced by dickite crystals with blocky habit reflecting a dissolution-precipitation mechanism. In most cases, the burial depth and temperature are considered to be the main parameters controlling the reaction. Moreover, the formation of dickite is associated with an increase in the activity of H^+, mosty related to the flux of acidic fluids derived from the maturation of organic matter (Sommer, 1975; Morad *et al.*, 1994; Van Keer *et al*, 1998).

Linking the morphological changes to crystal-structure data obtained by combined analytical techniques resulted in more detailed interpretations of the dickite formation mechanism, mainly from a kaolinite precursor (Ruiz-Cruz and Moreno-Real, 1993; Lanson *et al.*, 1996; Beaufort *et al.*, 1998). A conversion *via* mixed-layer kaolinite-dickite was suggested by Ruiz-Cruz and Moreno-Real (1993). Lanson *et al.* (1996) noted a gradual increase in kaolinite crystallinity without significant morphological changes and suggested a solid-state transformation to kaolinite with better crystal structure prior to its conversion to dickite. Based on a study of several size fractions, Beaufort *et al.* (1998) concluded that the early diagenetic and fine kaolinite is progressively transformed into dickite with a gradual increment in structural order and crystal size, establishing a schematic reaction model related to burial depth. The transformation is concomitant with the transition from booklet to blocky morphology and takes place at burial depths between 2500 and 5000 m in the North Sea (Beaufort *et al.*, 1998). At that burial depth, precipitation of dickite proceeds *via* dissolution of fine kaolinite crystals as well as directly by alteration of detrital feldspar and mica grains (Lanson *et al.*, 2002).

The Permo-Triassic fluvial red beds from the SE Iberian Range (NE Spain) give way to a good example of an outcropping sequence where kaolin minerals occur extensively in coarse-grained sediments (Gómez-Gras, 1993b; Martín-Martín, 2004; Martín-Martín *et al.*, 2006). Those authors reported the presence of dickite and noted three main features differentiating the area from other case studies reported in the literature: (1) lack of a significant amount of feldspars in the original late

* E-mail address of corresponding author:
juandiegomartin@gmail.com
DOI: 10.1346/CCMN.2007.0550503

Permian and early Triassic sediments; (2) limited burial depth of the studied sedimentary succession (<2000 m); and (3) relatively high paleogeothermal gradients (~49ºC/km).

The aim of this work is to investigate the morphology and crystal structure of kaolin minerals in the Permo-Triassic sandstones in order to point out the extensive dickitization recorded in the sedimentary succession. Moreover, the formation of dickite is linked to the tectonic and thermal evolution of the Iberian Range.

GEOLOGICAL SETTING

Location and structure of the study area

The Iberian Range is an intracratonic fold-thrust belt that resulted from the Paleogene inversion of the NW–SE trending Iberian Basin (Guimerà and Álvaro, 1990). The Iberian Basin developed between late Permian and late Cretaceous as a result of the widespread extension that affected the Iberian Plate during the opening of the Alpine Tethys and North Atlantic (Salas *et al.*, 2001). Two major rifting stages have been recognized (late Permian–Triassic and late Jurassic–early Cretaceous) followed by two post-rift thermal subsidence stages (Salas and Casas, 1993). Deposition of the Permo-Triassic red beds took place during the first stage of rifting in half-graben basins (Arche and López-Gómez, 1992; Gómez-Gras, 1993a).

The studied outcrops represent the NE margin of the Permo-Triassic Iberian Basin and are presently located in the south-eastern part of the Iberian Range (NE Spain) (Figure 1a). The structure of the area is characterized by a system of NE–SW oriented listric faults that bring to outcrop the Hercynian basement, Permian and Triassic, and a thin Jurassic and Cretaceous cover (Roca *et al.*, 1994) (Figure 1b).

Permo-Triassic lithostratigraphy

The post-Hercynian sedimentary pile is <2000 m thick and unconformably overlies deformed Carboniferous rocks comprising slates and greywackes with sporadic beds rich in plant remains (Sos, 1975). The Permo-Triassic sediments cover the post-Hercynian unconformity and form a succession of continental red beds up to 490 m thick (Figure 2), which is divided into three lithological formations (Arche and López-Gómez, 1992). These formations are referred to as late Permian (Alcotas Fm.), early Triassic (Cañizar Fm.) and Middle Triassic (Eslida Fm.) in order to facilitate the discussion. The late Permian is 335 m thick and is formed by sandstones, siltstones and mudstones interpreted as floodplain deposits of low sinuosity, ephemeral rivers and temporary lakes (Arche and López-Gómez, 1992; Gómez-Gras, 1993b). The base of the late Permian succession is a conglomeratic level deposited as alluvial fans deriving from the Hercynian highlands. Frequent coalified wood fragments occur in the base of the sandstones in the first half of the late Permian succession. The early Triassic (125 m thick) is composed of pink to red colored sandstones with minor conglomerates and scarce mudrocks, interpreted as braided river deposits (Arche and López-Gómez, 1992; Gómez-Gras, 1993b). The Middle Triassic is 30 m thick and is made up of mudstones, siltstones and sandstones interpreted as floodplain deposits of low sinuosity rivers (Arche and López-Gómez, 1992; Gómez-Gras, 1993b). The Permo-Triassic succession is overlain by the Muschelkalk limestones (López-Gómez and Arche, 1992).

Detrital and clay mineral composition of sandstones

Late Permian and early Triassic sandstones are sublitharenites that evolve upwards to quartz-arenites (Gómez-Gras, 1993b) (Figure 3). Late Permian sand-

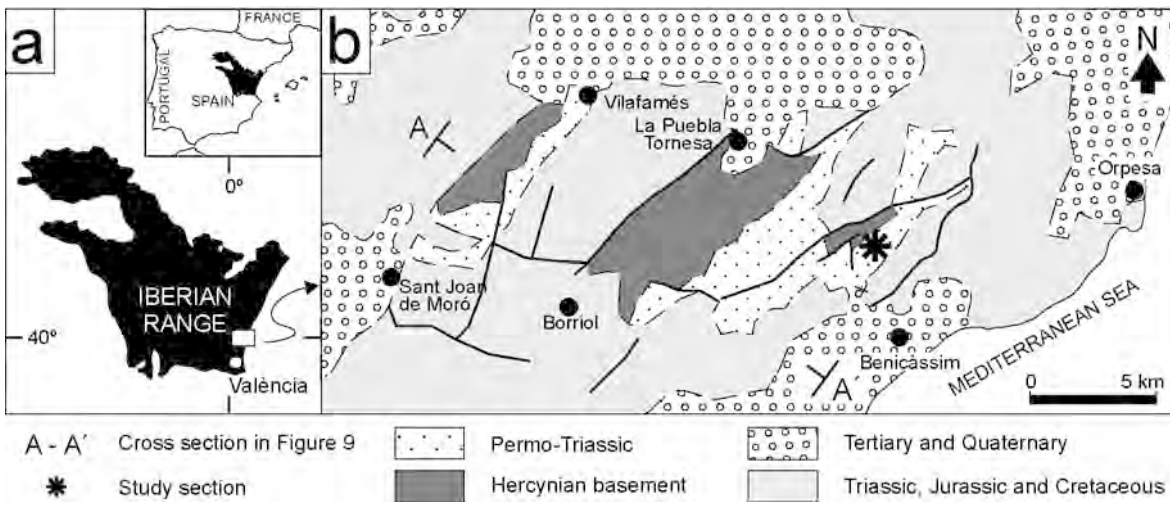

Figure 1. (a) Location map showing the Iberian Range in NE Spain. (b) Simplified geological map of the study area showing the location of Les Agulles section.

https://doi.org/10.1346/CCMN.2007.0550503 Published online by Cambridge University Press

stones are fine-grained whereas those of the early Triassic are mainly medium-grained. Quartz is the dominant component, forming between 60 and 72% of the sandstones (Gómez-Gras, 1993b). Other important components include metamorphic rock fragments (<8%) and chert (<2%), whereas minor amounts of intrabasinal fragments, muscovite and heavy minerals occur also. Feldspars, which are dominated by plagioclase, are rare and mostly altered. Clay minerals (1–8%) have been formed by the alteration of detrital mica and feldspars. Middle Triassic sandstones are very fine-grained litharenites (Gómez-Gras, 1993b). X-ray diffraction (XRD) analysis of sandstones revealed a clay mineral assemblage formed by illite and kaolin minerals, accompanied in the basal late Permian beds by trace to minor amounts of chlorite and mixed-layer illite-smectite (I-S) (Martín-Martín, 2004). The lack of significant amounts of feldspars in late Permian and early Triassic deposits from the SE Iberian Range is associated with the weathering of the Hercynian basement from the provenance area (Gómez-Gras, 1993b; Martín-Martín, 2004).

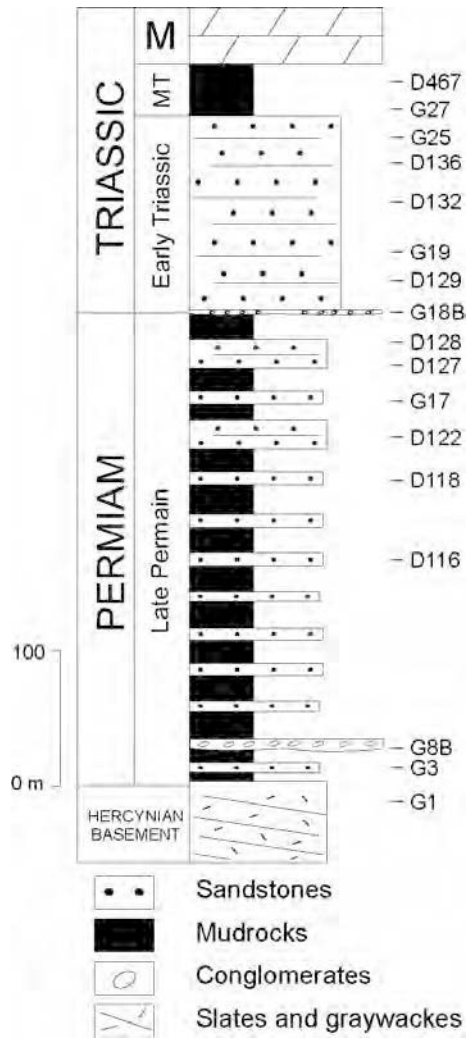

Figure 2. Synthetic lithological section of the Permo-Triassic sequence from the study area showing the occurrence of interbedded sandstones and mudrocks. MT: Middle Triassic; M: Muschelkalk.

SAMPLES AND METHODS

Seventeen samples distributed throughout the Permo-Triassic succession have been collected from the Les Agulles section outcropping in the Desert de les Palmes area (Figures 1 and 2). Thin-sections were analyzed in a conventional polarizing microscope in order to establish the paragenetic sequence of diagenetic alterations. Additionally, detailed analysis of size and morphology of kaolin minerals was carried out using a Leo 440i scanning electron microscope (SEM) equipped with a Link-Oxford energy dispersive X-ray (EDX) spectrometer. Observations were conducted on freshly fractured and gold-coated rock fragments.

In order to evaluate the occurrence of dickite along the Permo-Triassic section, five representative samples were selected on the basis of: (1) kaolin mineral content, and (2) position in the lithostratigraphical succession. These samples include sandstone and conglomerate beds (Figure 2). Four size fractions (<1 μm, <2 μm, <6.3 μm and <20 μm) were extracted from each of the selected samples by successive dispersion and sedimentation cycles. The morphology and crystal structure of kaolin-type minerals were examined in the four size fractions by means of complementary analytical techniques as recommended by Lanson *et al.* (2002).

The XRD analyses were performed on randomly oriented powders using a Siemens D5000 diffractometer equipped with monochromatic CuKα radiation.

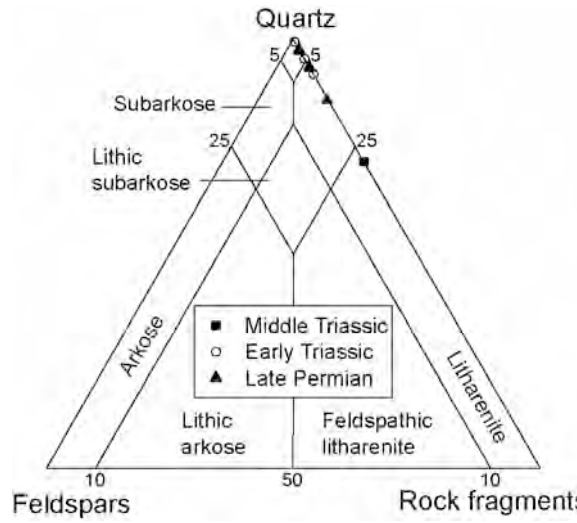

Figure 3. Detrital composition of the studied sandstones plotted on McBride's classification diagram showing the lack of feldspars in the Permo-Triassic succession (data from Gómez-Gras, 1993b).

https://doi.org/10.1346/CCMN.2007.0550503 Published online by Cambridge University Press

Measurements were made in the 19–40º2θ range with a scanning step size of 0.02º2θ and a counting time of 10 s per step. Identification of kaolin minerals was performed using non-basal reflections (Bailey, 1980; Drits and Tchoubar, 1990). The kaolin minerals/illite ratio was estimated from XRD patterns obtained from oriented preparations (air-dried and glycolated) of each size fraction. Measurements were made in the 2–30º2θ range with a scanning step size of 0.02º2θ and a counting time of 1 s per step. Abundances of kaolin minerals and illite were estimated following Caballero and Martín-Vivaldi (1975).

Fourier transform infrared (FTIR) spectroscopy spectra were recorded from specimens embedded in KBr pellets (2 wt.% sample) using a Nicolet spectrometer (20SXB) equipped with a deuterated triglycine sulfate (DTGS) infrared detector. The range analyzed was 4000–400 cm^{-1} and the resolution was 2 cm^{-1}. Up to 300 scans were accumulated in order to improve the signal to noise in the spectra. The identification of kaolin minerals is documented by analysis of the hydroxyl-stretching bands in the 3800–3500 cm^{-1} region of the spectra (Russell, 1987).

Differential thermal analysis (DTA) and thermogravimetry (TG) were carried out on a Mettler-Toledo 851e analytical system. Curves were obtained from 35 mg samples heated at rate of 10ºC/min from 25 to 1100ºC. Diagnostic dehydroxylation endothermic effects for kaolinite and dickite are considered to be at ~525ºC and ~680ºC, respectively (Mackenzie, 1970). Dehydroxylation effects of kaolin minerals are associated with a weight loss in TG analysis corresponding to the reaction (Paterson and Swaffield, 1987):

$$Al_2Si_2O_5\ (OH)_4 \rightarrow Al_2Si_2O_7 + 2H_2O$$

The thermal evolution of the studied samples is shown in derivative thermogravimetric (DTG) curves as weight loss effects are more obvious than the equivalent dehydroxylation effects from differential thermal analysis (DTA).

EXPERIMENTAL RESULTS

Petrographic observations

Kaolin minerals occur mainly as crystal aggregates that fill intergranular pores or replace muscovite, feldspars and mud intraclast (Figure 4). Kaolinitization of muscovite is particularly extensive in the early Triassic sandstones, showing a complete gradation between partially to totally altered mica (pseudomorphs). Large kaolin mineral aggregates with typical accordion-like shape show unaltered sheets of parent muscovite grains demonstrating an origin related to replacement and expansion of mica flakes into adjacent pore space (Figure 4b). Very coarse kaolin mineral aggregates with fan-like shape are also seen (Figure 4c). Kaolin mineral pseudomorphs of feldspars are also present although quantitatively insignificant.

Examination by SEM revealed the presence of pore-filling kaolin minerals with a large range of crystal sizes (Figure 5). Very small crystals (<1 μm) occur as pseudo-

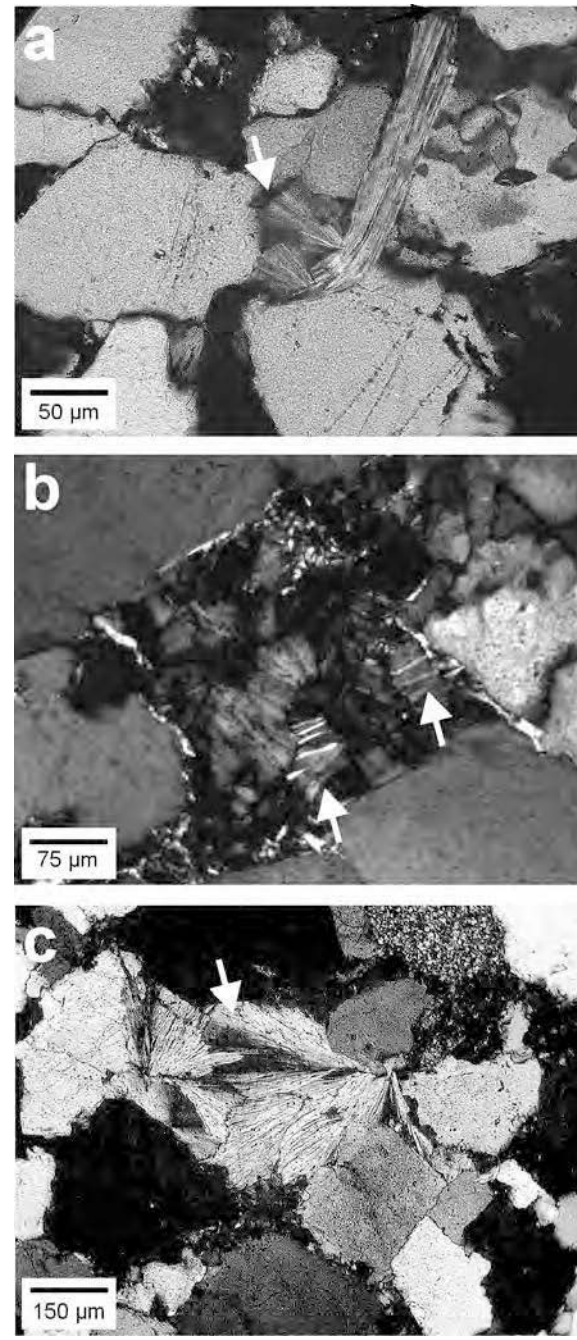

Figure 4. Photomicrographs (crossed nicols) showing partially to totally kaolinitized mica. (a) Muscovite partially altered to kaolin minerals (white arrow) (Sample G25). (b) Large kaolin mineral aggregates (accordions) showing unaltered sheets of parent muscovite grains (white arrow) (Sample G17). (c) Very coarse kaolin mineral (dickite) aggregates with fan-like shape (white arrow) (Sample G19).

https://doi.org/10.1346/CCMN.2007.0550503 Published online by Cambridge University Press

hexagonal individual platelets, whereas crystals >1 μm typically form booklets composed of pseudo-hexagonal stacked plates (Figure 5a–c). In these stacks, crystals with thick and blocky habit are frequently intercalated with thinner crystals (Figure 5c). As the size fraction increases, a progressive thickening of the booklets occurs concomitantly with thickening of the plates stacked along the c^* axis. The largest booklets are composed exclusively of blocky crystals which are elongated (10 to 15 μm) in the direction of the *ab* plane and up to 2 μm thick along the c^* axis (Figure 5d).

The fine kaolin minerals appear, in turn, slightly altered to lath-shaped illite as suggested by the partial dissolution and etched plates (Figure 5e). Conversely,

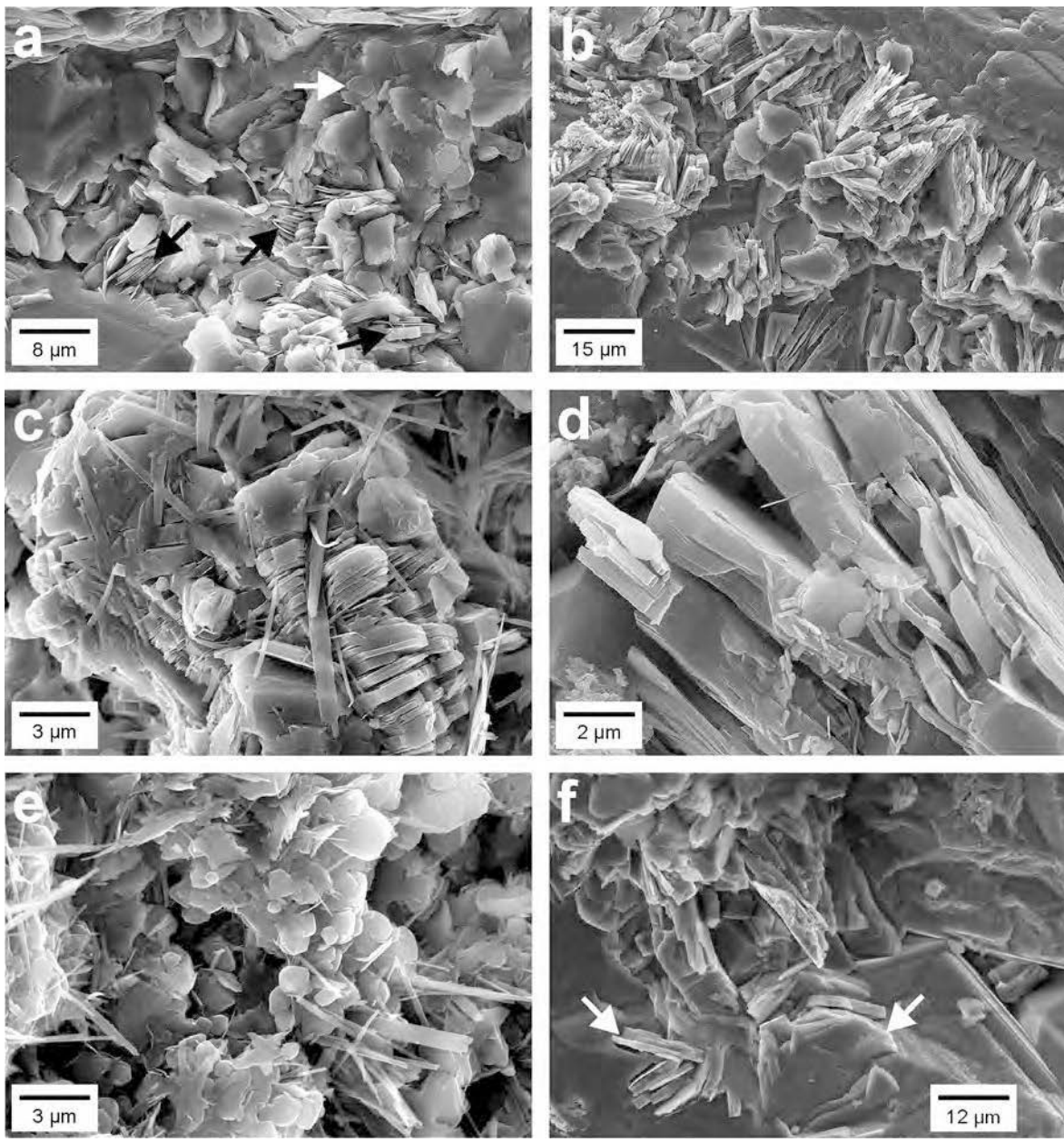

Figure 5. SEM images of kaolin minerals. (a) Thin kaolin mineral (dickite and kaolinite?) plates with crystal size ~2 μm. Note the small etched plates (white arrows) coexisting with well developed and thick crystals (black arrows) (Sample G19). (b) Booklets of kaolin minerals (dickite) completely closing the pore space (sample G18B). (c) Kaolin mineral (dickite) booklet composed of plates with different thicknesses along the c^* axis and covered by authigenic lath-shaped illite (sample G18B). (d) Very coarse kaolin mineral (dickite) booklet comprising blocky pseudohexagonal plates up to 2 μm thick along the c^* axis (sample G25). (e) Very fine kaolin minerals (kaolinite) altered to illite showing dissolution features (etched plates) (sample G8B). (f) Kaolin mineral (dickite) plates engulfed by quartz overgrowths (sample G25).

https://doi.org/10.1346/CCMN.2007.0550503 Published online by Cambridge University Press

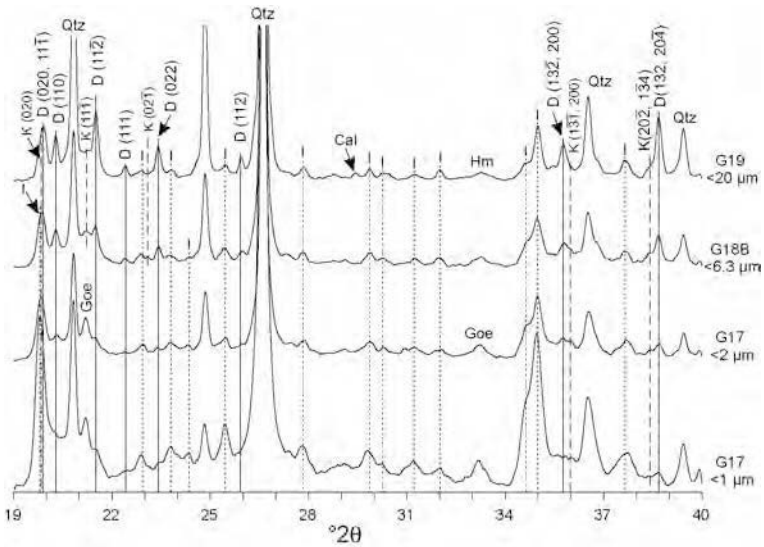

Figure 6. XRD patterns of the four size fractions showing the dominant occurrence of kaolin minerals and illite. Characteristic *hkl* reflections of dickite (solid line), kaolinite (dashed line) and illite (dotted line) are indicated (Bailey, 1980). Qtz: quartz, Cal: calcite, Goe: goethite, Hm: hematite. CuKα radiation.

the thick and well developed crystals appear unaltered but also covered by illite (Figure 5c). Thus, illite formation occurred after the growth of any kaolin minerals. Kaolin minerals are frequently engulfed by quartz overgrowths demonstrating the earlier formation of the former (Figure 5f).

X-ray diffraction

The XRD analysis of the four size fractions obtained from randomly oriented powders reveals the predominance of dickite in all the samples, whereas kaolinite is rarely recognized. Characteristic dickite reflections are distinguished in size fractions coarser than <2 µm, being noted at 4.44 Å (020,11$\bar{1}$), 4.36 Å (110), 4.12 Å (11$\bar{2}$), 3.95 Å (111), 3.79 Å (022), 3.42 Å (112), 2.50 Å (13$\bar{2}$,200) and 2.324 Å (132,20$\bar{4}$) (Figure 6). These reflections become prominent as the size fraction increases, proving the occurrence of larger amounts of dickite in the coarser fractions. Together with dickite, the presence of kaolinite in the <6.3 µm and/or <20 µm size fractions of some samples is suggested by weak reflections at 4.46 Å (020), 4.18 Å (11$\bar{1}$), 3.84 Å (02$\bar{1}$), 2.49 Å (1$\bar{3}$1) and 3.34 Å (20$\bar{2}$,1$\bar{3}$1) (Figure 6). Conversely, kaolin minerals are recognized in the finer size fractions where illite is the dominant clay mineral. Reflections of kaolin minerals in the finer size fractions are presumably masked due to the overlap with those of illite and non-clay minerals such as quartz and goethite (Figure 6). Illite reflections correspond dominantly to the $2M_1$ polytype, reflecting the dominance of detrital clay mica in the samples.

Quantification of the clay components from analysis of the XRD oriented preparations also shows that illite is the dominant clay component in the finer size fraction and decreases progressively towards the coarsest fraction, whereas the kaolin minerals content increases notably (Table 1).

Fourier transform infrared spectroscopy

The IR spectra of the four size fractions show three strong absorptions bands in the hydroxyl-stretching region (3700−3600 cm^{-1}) centered at 3621, 3649 and 3701 cm^{-1} (Figure 8). The position and relative intensity of these bands indicate that considerable

Table 1. Clay mineral composition of selected samples.

Sample	Fraction	K (%)	I (%)
G25	<1 µm	37	63
	<2 µm	60	40
	<6.3 µm	77	23
	<20 µm	90	10
G19	<1 µm	33	67
	<2 µm	52	48
	<6.3 µm	72	28
	<20 µm	81	19
G18B	<1 µm	24	76
	<2 µm	52	48
	<6.3 µm	69	31
	<20 µm	75	25
G17	<1 µm	24	76
	<2 µm	42	58
	<6.3 µm	59	41
	<20 µm	78	22
G8B	<1 µm	23	77
	<2 µm	34	66
	<6.3 µm	37	63
	<20 µm	59	41

K: kaolin minerals; I: illite

https://doi.org/10.1346/CCMN.2007.0550503 Published online by Cambridge University Press

amounts of dickite are present in all size fractions. Nevertheless, the asymmetry of the 3701 cm^{-1} band and a shoulder at ~3670 cm^{-1} also suggest the occurrence of small amounts of kaolinite. A high ratio of illite in the four size fractions, as detected by XRD, is noted by the broad 3620 cm^{-1} band. The definition of this band, however, increases as the amount of illite decreases from the finer to the coarsest size fraction (Figure 7; Table 1).

Differential thermal analysis and thermogravimetry

The DTA curves of the finer size fractions are poor in quality and frequently the thermal behavior is difficult to constrain. When coupled with DTG curves, however, the associated weight loss and also the maximum temperatures at which the effects took place are better achieved (Figure 8).

The DTG curves of the <1 and <2 μm size fractions show broad weight loss effects centered around 535 and 545ºC, respectively. These effects are related to the large amount of illite in the finer size fractions, as noted previously by XRD and FTIR, and the probable contribution of kaolinite (Paterson and Swaffield, 1987). Moreover, its broadening towards high temperatures and a shoulder at 625ºC suggest the existence of poorly ordered dickite in these size fractions too. Progressive shifting of the main weight loss effect towards higher temperatures (~600ºC) with increasing size fraction reflects the decrease in the amount of illite in the coarser fractions and the dominance of kaolin minerals, mostly dickite. Kaolin minerals form shoulders to well individualized peaks between 640 and 670ºC in the <6.3 μm size fraction, suggesting the presence of dickite crystals with varying degrees of structural ordering. A single peak centered at 670ºC in the DTG pattern of the <20 μm size fraction indicates the presence of well ordered dickite in the coarsest size fraction.

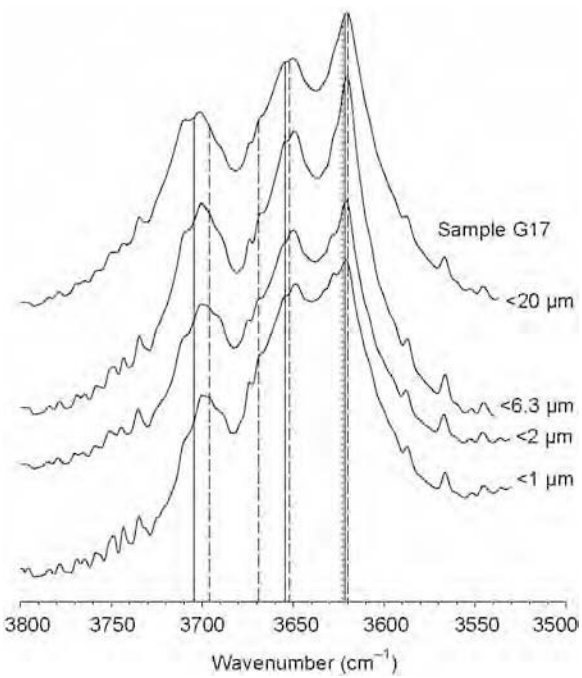

Figure 7. IR spectra of the four size fractions showing characteristic kaolin minerals and illite bands in the OH-stretching region (sample G17). Theoretical lines of dickite (solid line), kaolinite (dashed line) and illite (dotted line) bands are noted (Russell, 1987).

DISCUSSION

Occurrence of kaolinite and dickite

The analytical results indicate that dickite with varying degrees of structural order is the dominant kaolin mineral in all the size fractions (Figures 4–8). Dickite is typically represented by booklets of pseudo-hexagonal stacked plates with variable thickness along the *c** axis. Moreover, very thick dickite crystals with blocky habit and well ordered structures are found in the coarsest size fractions (Figure 5d). Kaolinite is not detected unambiguously in the sandstones studied although it presumably concentrates in the finer size fractions and forms thinner

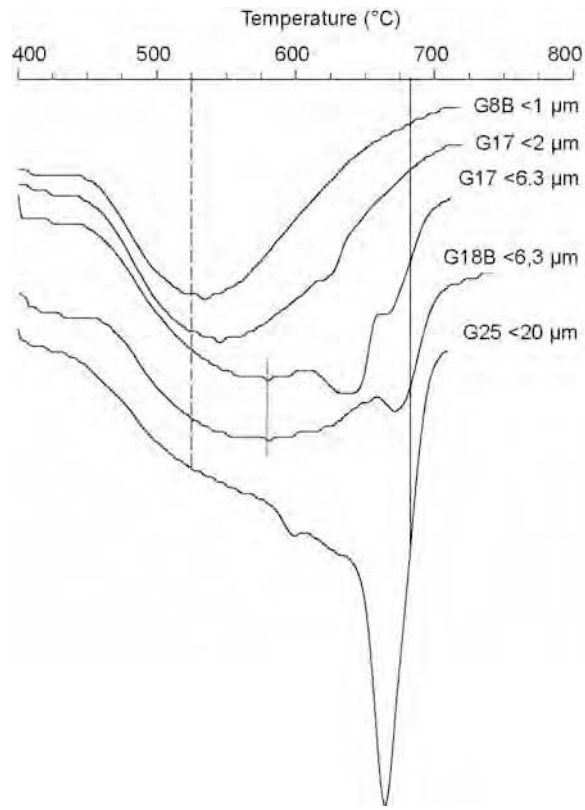

Figure 8. DTG (derivative themogravimetric) curves of sandstone samples showing the occurrence of intermediate weight loss (endotherms) effects between kaolinite and dickite diagnostic temperatures. The diagnostic dehydroxylation temperatures of dickite (solid line), kaolinite (dashed line) and quartz (dotted line) are noted (Mackenzie, 1970).

https://doi.org/10.1346/CCMN.2007.0550503 Published online by Cambridge University Press

crystals than dickite (Ehrenberg *et al.*, 1993; Beaufort *et al.*, 1998). The presence of kaolinite in the <6.3 and <20 μm size fractions, however, is interpreted to result either from a deficient sample dispersion process or the presence of kaolinitized mica fragments in the coarse fractions (Figure 4).

The problems in identifying kaolin minerals by XRD patterns are attributed, at least in part, to the large amount of illite observed in the Permo-Triassic sandstones (Table 1). Unlike dickite, the illite content increases with decreasing size fraction preventing an accurate identification of kaolin minerals in the finer size fractions. Difficulties in discriminating kaolin mineral polymorphs by XRD have previously been related to both the interference of clay and non-clay minerals (Ehrenberg *et al.*, 1993), and the presence of kaolin minerals with different degrees of ordering (Brindley and Porter, 1978; Beaufort *et al.*, 1998).

According to the computer-generated IR spectra reported by Ehrenberg *et al.* (1993), the relative intensity between the three strongest absorption bands in the OH-stretching region suggest a high dickite/kaolinite ratio (Figure 7). In agreement with the XRD data, the IR results reflect the nearly exclusive occurrence of dickite in the coarsest size fractions. Taking into account the quantitative data reported by Ehrenberg *et al.* (1993), the percentages of dickite up to 80−100% are estimated for the coarsest size fractions whereas the large amount of illite precludes estimation in the finer fractions.

Accurate data for structural ordering is obtained from DTA-TG experimental results. The gradual shifting of the dehydroxylation/weight loss effects towards higher temperatures as size fraction increases reflects the progressive improvement in the structural order of dickite with increasing crystal size (Figure 8). Therefore, the intermediate endotherms/weight loss effects between kaolinite and dickite diagnostic temperature observed in the DTA-DTG curves are interpreted to result from the presence of dickite with varying degrees of structural disorder (Brindley and Porter, 1978; Beaufort *et al.*, 1998).

Origin and time of dickite formation

Petrographic observations suggest that the alteration of fine kaolin crystals, probably kaolinite, and detrital mica grains provide material to form dickite aggregates in adjacent intergranular pores. The presence of kaolinite, together with the improvement in the structural order of dickite crystals as size fraction increases, indicate that the transformation of the early kaolinite into dickite was associated with an increase in crystal size, as previously observed by several authors (*e.g.* Beaufort *et al.*, 1998). Consequently, the formation of dickite was accomplished by a dissolution-precipitation process that resulted in coarse and blocky crystal habits (Jourdan *et al.*, 1987; Ehrenberg *et al.*, 1993; McAulay *et al.*, 1994; Beaufort *et al.*, 1998).

The reported kaolin mineral accordion-like aggregates are typically associated with the early diagenetic kaolinitization and expansion of detrital mica (Bjørlykke and Brendsdal, 1986; De Ros, 1998). Hence, dickite is interpreted to result at least in part from the dissolution of previously kaolinitized muscovite grains (pseudomorphs) although direct precipitation from a mica precursor is not ruled out (Lanson *et al.*, 2002). The occurrence of very coarse dickite aggregates with fan-like shape under optical microscope probably represents the last stage of a kaolinitized mica recrystalization (Figure 4c). A contribution by the alteration of feldspars to dickite is insignificant due to the small amount of feldspars recorded in the sandstones studied.

The formation of dickite has been reported to be facilitated by the decrease in pH of formation waters resulting from the flux of acids during the maturation of organic matter (Sommer, 1975; Van Keer *et al*, 1998). A probable source of such fluids in the area studied is the underlying Carboniferous rocks, which had been connected laterally to the studied sequence since the early stages of rifting (Roca *et al.*, 1994) (Figures 1, 9). Alternatively, organic acids can be derived from the coalified wood fragments located in the base of sandstone beds within the late Permian succession. Fluid flow was probably enhanced by the system of NE−SW listric faults, located at the present day at a depth of 1.7−2.2 km, resulting from the extensional tectonic regime associated with the rifting (Roca and Guimerà, 1992) (Figure 9).

The crystalline morphology and the improvement of the structural ordering of dickite observed are in good agreement with the idealized schematic evolution of kaolin minerals with increasing burial proposed by Beaufort *et al.* (1998) and modified by Lanson *et al.* (2002). In the studied sandstones, however, the dickitization process took place at a burial depth notably lower (<2000 m) (Roca *et al.*, 1994).

Petrographic examination revealed that kaolin illitization post-dates dickite formation, both process representing late diagenetic conditions (Worden and Morad, 2002). However, the maximum thickness of the sedimentary cover over the post-Hercynian unconformity is estimated to have been <2 m during the late Cretaceous thermal post-rift (Roca *et al.*, 1994). Vitrinite reflectance analysis of late Permian coal samples indicates a maximum burial temperature of ~118ºC, which represents a paleogeothermal gradient of ~49ºC/km (Martín-Martín *et al.*, 2006). Consequently, the high paleogeothermal gradient is considered to be the main factor controlling the extensive formation of dickite in the Permo-Triassic sandstones studied. The origin of such a relatively high heat flow is probably related to the extensional fault system affecting the Hercynian basement described above (Figure 9). The occurrence of a regional high heat flow in the area is also seen in the very low metamorphic conditions registered in the Permo-Triassic succession

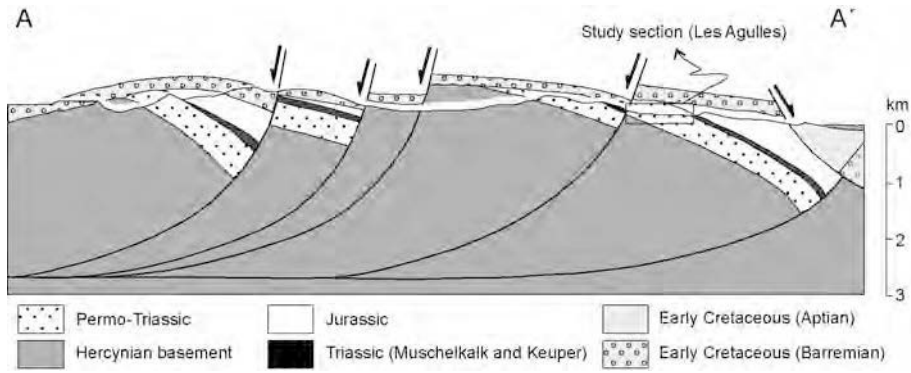

Figure 9. Cross-section showing the structural framework of the study area (modified after Roca *et al.*, 1994). See Figure 1 for location.

from the basin depocenter, presumably related to late Cretaceous times (Salas *et al.*, 2005). The maximum temperature recorded in the Permo-Triassic succession is in good accord with the range of burial temperatures (80–120ºC) estimated for the formation of dickite in the North Sea (*e.g.* Ehrenberg *et al.*, 1993; McAulay *et al.*, 1994).

Illitization of kaolin minerals is reported to be a common process at temperatures >70ºC (Worden and Morad, 2002). Hence, the slight to absent transformation of kaolin minerals into illite in the studied rocks is attributed to the lack of detrital K-feldspars and/or an external source of K^+ (Berger *et al.*, 1997). The alteration of detrital mica and mud intraclasts are considered to be the main source of K^+ for the formation of authigenic illite from a kaolin mineral precursor (Martín-Martín *et al.*, 2006). Additionally, the dominance of the dickite polymorph may also be a limiting factor for kaolin mineral illitization due to its better ordered crystal structure than kaolinite (Morad *et al.*, 1994).

CONCLUSIONS

Study of four size fractions of the Permo-Triassic sandstones from the SE Iberian Range (Spain) reveals that dickite with varying degrees of structural order-disorder is the dominant kaolin mineral in the range <1 μm to <20 μm. Hence, our results reflect the nearly complete dickitization of the presumably early diagenetic kaolinite.

The morphological changes and the increase in the structural order of kaolin minerals noted with increasing size fraction suggest a mechanism of dissolution-precipitation for dickite formation. Together with the recrystallization of the fine kaolin minerals, dickite growth was facilitated by the dissolution of kaolinitized muscovite grains as well as by direct precipitation from a mica precursor. The participation of feldspars in the process is irrelevant due to the small amount of feldspar present in the original mineralogy of the sandstones studied.

Extensive dickitization of the Permo-triassic sandstones at burial conditions shallower than those generally reported in the literature is attributed to the high paleogeothermal gradient which affected the SE Iberian Basin during the late Cretaceous post-rift thermal stage.

ACKNOWLEDGMENTS

J.D. Martín-Martín thanks Generalitat Valenciana (Spain) for a post-doc fellowship at Uppsala University (CTBPDC/2004/069). The research was partially supported by the Spanish Ministry of Education and Science (Project BTE2003-06915) and (CGL2005-07445-C03-01/BTE). The authors thank R. Salas (Barcelona University) for discussions and data on the SE Iberian Range structural framework. A critical review by S. Morad helped to improve the manuscript. S. Ehrenberg, Associate Editor B. Lanson, and an anonymous reviewer are acknowledged for their critical and constructive comments.

REFERENCES

Arche, A. and López-Gómez, J.L. (1992) Una nueva hipótesis sobre las primeras etapas de la evolución tectosedimentaria de la cuenca pérmico-triásica del SE de la Cordillera Ibérica. *Cuadernos de Geología Ibérica*, **16**, 115–143.

Bailey, S.W. (1980) Structures of layer silicates. Pp. 249–303 in: *Crystal Structures of Clay Minerals and their X-ray Identification* (G.W. Brindley and G. Brown, editors). Monograph **5**, Mineralogical Society, London.

Beaufort, D., Cassagnabere, A., Petit, S., Lanson, B., Berger, G., Lacharpagne, J.C. and Johansen, H. (1998) Kaolinite-to-dickite reaction in sandstone reservoirs. *Clay Minerals*, **33**, 297–316.

Berger, G., Lacharpagne, J.C., Velde, B., Beaufort, D., Cassagnabere, S. and Lanson, B. (1997) Kinetic constraints on illitization reactions and the effects of organic diagenesis in sandstone/shale sequences. *Applied Geochemistry*, **12**, 23–35.

Bjørlykke, K. and Brendsdal, A. (1986) Diagenesis of the Brent sandstone in the Statfiord Field, North Sea. Pp. 157–167 in: *Roles of Organic Matter in Sediment Diagenesis* (D.L. Gautier, editor). Special Publication **47**, SEPM, USA.

Brindley, G.W. and Porter, A.R. (1978) Occurrence of dickite in Jamaica – ordered and disordered varieties. *American Mineralogist*, **63**, 554–562.

Caballero, M.A. and Martín-Vivaldi, J.L. (1975) *Estudio mineralógico y genético de la fracción fina del trías*

https://doi.org/10.1346/CCMN.2007.0550503 Published online by Cambridge University Press

español. Memoria del Instituto Geológico y Minero de España. Servicio de Publicaciones Ministerio de Industria, Madrid, 277 pp.

De Ros, L.F. (1998) Heterogeneous generation and evolution of diagenetic quartz-arenites in Silurian-Devonian Furnas Formation of the Paraná Basin, southern Brazil. *Sedimentary Geology*, **116**, 99–128.

Drits, V. and Tchoubar, C. (1990) The modelization method in the determination of the structural characteristics of some layer silicates: Internal structure of the layers, nature and distribution of the stacking faults. Pp 233–303 in: *X-ray Diffraction by Disordered Lamellar Structures* (V. Drits and C. Tchoubar, editors). Springer-Verlag, Berlin.

Ehrenberg, S.N., Aagaard, P., Wilson, M.J., Fraser, A.R. and Duthie, D.M.L. (1993) Depth-dependent transformation of kaolinite to dickite in sandstones of the Norwegian continental shelf. *Clay Minerals*, **28**, 325–352.

Gómez-Gras, D. (1993a) El Permotrías de la Cordillera Costero Catalana: Facies y Petrología Sedimentaria (Parte I). *Boletín Geológico y Minero*, **104**, 115–161.

Gómez-Gras, D. (1993b) El Permotrías de las Baleares y de la vertiente mediterránea de la Cordillera Ibérica y del Maestrat: Facies y Petrología Sedimentaria (Parte II). *Boletín Geológico y Minero*, **104**, 467–515.

Guimerà, J. and Álvaro, M. (1990) Structure et évolution de la compression alpine dans la Chaîne ibérique et la Chaîne côtiere catalane (Espagne). *Bulletin de la Societé Géologique de France*, **VI**, 339–348.

Jourdan, A., Thomas, M., Brevart, O., Robson, P., Sommer, F. and Sullivan, M. (1987) Diagenesis as the control of the Brent sandstones reservoir properties in the Greater Alwyn area (East Shetland Basin). Pp. 951–961 in: *Petroleum Geology of North West Europe* (J. Brooks and K. Glennie, editors). Proceedings of the 3rd Conference on Petroleum Geology of North West Europe.

Lanson, B., Beaufort, D., Berger, G., Baradat, J. and Lacharpagne, J.C. (1996) Illitization of diagenetic kaolinite-to-dickite conversion series: late-stage diagenesis of the lower Permian Rotliegend sandstones reservoir, offshore of the Netherlands. *Journal of Sedimentary Research*, **66**, 501–518.

Lanson, B., Beaufort, D., Berger, G., Bauer, A., Cassagnabère, A. and Meunier, A. (2002) Authigenic kaolin and illitic minerals during burial diagenesis of sandstones: a review. *Clay Minerals*, **37**, 1–22.

López-Gómez, J.L. and Arche, A. (1992) Paleogeographical significance of the Röt (Anisian, Triassic) Facies (Marine clays, muds and marls Fm.) in the Iberian Ranges, eastern Spain. *Palaeogeography, Palaeoclimatology, Palaeoecology*, **91**, 347–361.

Mackenzie, R.C. (1970) Simple phyllosilicates based on gibbsite- and brucite-like sheets. Pp. 497–537 in: *Differential Thermal Analysis*. (R.C. Mackenzie, editor). Academic Press, New York.

Martín-Martín, J.D. (2004) Los minerales de la arcilla del Permo-Triásico de la Cordillera Ibérica oriental: Procedencia y evolucion diagenética. PhD thesis, Universidad Jaume I, Castelló, Spain, 189 pp.

Martín-Martín, J.D., Gómez-Gras, D., Sanfeliu, T., Permanyer, A., Nuñez, J.A. and Parcerisa, D. (2006) Conditions of kaolin illitization in the Permo-Triassic sandstones and conglomerates from the SE Iberian Ranges, Spain. *Journal of Geochemical Exploration*, **89**, 263–266.

McAulay, G.E., Burley, S.D., Fallick, A.E. and Kusznir, N.J. (1994) Palaeohydrodynamic fluid flow regimes during diagenesis in the Brent Group in the Hutton-NW Hutton reservoirs: constraints from oxygen isotope studies of authigenic kaolin and reverse flexural modeling. *Clay Minerals*, **29**, 609–626.

Morad, S., Ben Ismail, H.N., De Ros, L.F., Al-Aasm, I.S. and Serrhini, N.-E. (1994) Diagenesis and formation water chemistry of Triassic reservoir sandstones from southern Tunisia. *Sedimentology* **41**, 1253–1272.

Paterson, E. and Swaffield, R. (1987) Thermal Analysis. Pp. 97–132 in: *A Handbook of Determinative Methods in Clay Mineralogy* (M.J. Wilson, editor). Blackie, Glasgow, UK.

Platt, J.D. (1993) Controls on clay mineral distribution and chemistry in the early Permian Rotliegend of Germany. *Clay Minerals*, **28**, 393–416.

Roca, E. and Guimerà, J. (1992) The neogene structure of the eastern Iberian margin: structural constraints on the crustal evolution of the Valencia trough (Western Mediterranean). *Tectonophysics*, **203**, 203–218.

Roca, E., Guimerà, J. and Salas, R. (1994) Mesozoic extensional tectonics in the southeast Iberian Chain. *Geological Magazine*, **131**, 155–168.

Ruiz-Cruz, M.D. and Andreo, B. (1996) Genesis and transformation of dickite in Permo-Triassic sediments (Betic Cordilleras, Spain). *Clay Minerals*, **31**, 133–152.

Ruiz-Cruz, M.D. and Moreno-Real, L. (1993) Diagenetic kaolinite/dickite (Betic Cordilleras, Spain). *Clays and Clay Minerals*, **41**, 570–579.

Russell, J.D. (1987) Infrared methods. Pp. 133–173 in: *A Handbook of Determinative Methods in Clay Mineralogy* (M.J. Wilson, editor). Blackie, Glasgow, UK.

Salas, R. and Casas, A. (1993) Mesozoic extensional tectonics, stratigraphy and crustal evolution during the Alpine cycle of the eastern Iberian Basin. *Tectonophysics*, **228**, 33–55.

Salas, R., Guimerà, J., Mas, R., Martín-Closas, C., Melendez, A. and Alonso, A. (2001) Evolution of the Mesozoic Central Iberian Rift System and its Cainozoic inversion (Iberian Chain). Pp. 145–185 in: *Pery-Tethyan Rift/Wrench Basins and Passive Margins* (P.A. Ziegler, W. Cavazza, A.H.F. Robertson and S. Crasquin-Soleau, editors). Mémoires du Muséum National d'Histoire Naturelle (186), Paris.

Salas, R., Caja, M.A., Martín, J.D., Mas, R. and Permanyer, A. (2005) Mid-Late Cretaceous volcanism, metamorphism and the regional thermal event affecting the Northeastern Iberian basins (Spain). Pp. 55–58 in: *Global Events during the Quiet Aptian-Turonian Superchron*. Géologie Alpine. Série Spéciale "Colloques et excursions", Grenoble, France.

Sommer, F. (1975) Histoire diagénétique d'une série gréseuse de Mer du Nord. Datation de l'introduction des hydrocarbures. *Revue de l'Institut Français du Petrole*, **30**, 729–741.

Sos, V. (1975) Los terrenos del Periodo Carbonífero de la provincia de Castellón. *Boletín de la Real Sociedad Española de Historia Natural*, Volumen Extraordinario 1er Centenario de la Fundación de la Real Sociedad Española de Historia Natural, Trabajos Científicos en Geología, 419–435.

Van Keer, I., Muchez, Ph. and Viaene, W. (1998) Clay mineralogical variations and evolutions in sandstone sequences near a coal seam and shales in the Westphalian of the Campine Basin (NE Belgium). *Clay Minerals*, **33**, 159–169.

Worden, R.H. and Morad, S. (2002) Clay minerals in sandstones: controls on formation, distribution and evolution. Pp. 3–41 in: *Clay Mineral Cements in Sandstones* (R.H. Worden and S. Morad, editors). International Association of Sedimentologists Special Publication, **34**. Blackwell Publishing, Oxford, UK.

(*Received 7 October 2006; revised 6 July 2007; Ms. 1187; A.E. Bruno Lanson*)